

Revisiting the Relationship between Adaptive Smoothing and Anisotropic Diffusion with Modified Filters

Bumsub Ham, *Student Member, IEEE*, Dongbo Min, *Member, IEEE* and Kwanghoon Sohn, *Member, IEEE*

Abstract—The anisotropic diffusion has been known to be closely related to the adaptive smoothing and be discretized in a similar manner. This paper revisits a fundamental relationship between two approaches. It is shown that the adaptive smoothing and the anisotropic diffusion have different theoretical backgrounds by exploring their characteristics with the perspective of a normalization, an evolution step size and an energy flow. Based on this principle, the adaptive smoothing is derived from a second order partial differential equation (PDE), not a conventional anisotropic diffusion, via the coupling of Fick’s law with a generalized continuity equation where a ‘source’ or ‘sink’ exists, which has not been extensively exploited. We show that the ‘source’ or ‘sink’ is closely related to the asymmetry of an energy flow as well as the normalization term of the adaptive smoothing. It enables us to analyze behaviors of the adaptive smoothing such as the maximum principle and stability with a perspective of a PDE. Ultimately, this relationship provides new insights into application-specific filtering algorithm design. By modeling the ‘source’ or ‘sink’ in the PDE, we introduce two specific diffusion filters, the robust anisotropic diffusion (RAD) and the robust coherence enhancing diffusion (RCED), as novel instantiations which are more robust against the outliers than the conventional ones.

Index Terms—Adaptive smoothing, anisotropic diffusion, energy flow, normalization, generalized continuity equation, coherence enhancing diffusion.

I. INTRODUCTION

IN low-level vision problems, there is a need to smooth images, while preserving universal features such as edges or boundaries, in order to find structures embedded in images [1]. Linear smoothing averages all pixels evenly without incorporating the local topology, leading to blurred features. Over the last two decades, there have been many advances in nonlinear smoothing in which prior knowledge is leveraged for grouping with similar pixels only. There having been many types of nonlinear smoothing [2], [3], partial differential equation (PDE) based smoothing and kernel based smoothing have been widely used. The typical examples of the PDE

based smoothing are the anisotropic diffusion [4] and the total variation diffusion [5], [6], which are also related to the wavelet shrinkage and morphology [6], [7]. The most representative examples of the kernel based smoothing are the adaptive smoothing [8], [9], the bilateral filter [10], the mean-shift filter [11], and the non-local filter [12]. Nonlinear smoothing has been successfully applied to the image denoising [13], [14], segmentation [15], structure decomposition [1], optical flow estimation [16], and manifold smoothing [17].

Many researchers have made efforts to investigate a fundamental relationship between the PDE based smoothing and the kernel based smoothing [13], [17], [8], [12], [18], [19], [20], [21], [22], [23]. Saint-Marc *et al.* showed that the adaptive smoothing is equivalent to the anisotropic diffusion [8]. Barash also derived a relationship between the adaptive smoothing and the anisotropic diffusion, and showed that Saint-Marc’s results are not consistent [19]. He also verified that the bilateral filter [10] becomes a generalized formulation of the adaptive smoothing by introducing 5-D pixels. Simoncelli and Hany generalized a steerable filter, as a type of the adaptive filter, such that the orientation and magnitude of local structures can be captured and analyzed together [24]. Buades *et al.* showed an asymptotic behavior of neighborhood filters as the size of the neighborhood shrinks to zero, and proved that these filters are asymptotically equivalent to the anisotropic diffusion [13]. Singer *et al.* viewed the non-local filter as a diffusion process, and analyzed a relationship between the non-local filter and the random walk theory [20]. Elad showed how the bilateral filter is improved and extended upon for handling more sophisticated reconstruction problems [21]. In [22], it was shown that the bilateral filter is the particular case of the mean-shift filter and can be obtained by fixing the spatial kernel of the mean-shift filter at each iteration. Motivated by these works, Paris and Durand casted the bilateral filter into a signal processing framework [25]. The intensity range was quantized and sampled into a small set of channels, which is similar to the channel smoothing [18], so that the computational efficiency could be dramatically improved. Recently, Sevilla-Lara and Learned-Miller extended the channels from an intensity range to an arbitrary feature space, enabling the channel smoothing to be applicable to high-level vision fields such as tracking [26].

In this paper, a traditional relationship between the adaptive smoothing and the anisotropic diffusion is revisited. Reinterpreting two approaches in terms of a normalization, an evolution step size and an energy flow, we show that the

Manuscript received July 15, 2012; revised October 8, 2012; accepted October 17, 2012.

Copyright (c) 2012 IEEE. Personal use of this material is permitted. However, permission to use this material for any other purposes must be obtained from the IEEE by sending a request to pubs-permissions@ieee.org.

This work was supported by the National Research Foundation of Korea (NRF) grant funded by the Korea government (MEST) (No. 2012-0004995).

B. Ham and K. Sohn are with the School of Electrical and Electronic Engineering, Yonsei University, 134 Sinchon-dong, Seodaemun-gu, Seoul, 120-749, South Korea (e-mail: mimo@yonsei.ac.kr; khsohn@yonsei.ac.kr).

D. Min is with the Advanced Digital Sciences Center, Singapore. (e-mail: dongbo@adsc.com.sg).

adaptive smoothing is equivalent to the anisotropic diffusion only when special constraints are imposed. Specifically, the energy flow of adaptive smoothing is asymmetric, whereas that of anisotropic diffusion is always symmetric. Considering an asymmetric energy flow, we derive the adaptive smoothing from a second order PDE, not a conventional anisotropic diffusion, via the coupling of Fick's law with a generalized continuity equation where a 'source' or 'sink' exists, which has not been extensively exploited. Namely, the equivalence between the adaptive smoothing and the second order PDE with the 'source' or 'sink' is explicitly investigated. Based on this fact, it is shown that the normalization term used in the adaptive smoothing, a fundamental form of the weighted average filter [19], comes from the 'source' or 'sink' in the generalized continuity equation. We also show that the adaptive smoothing satisfies a maximum principle and is always stable with a perspective of a PDE. Furthermore, the proposed PDE gives us new diffusion filters such as the robust anisotropic diffusion (RAD) and the robust coherence enhancing diffusion (RCED).

The significance of our work is as follows: First, we distinguish the adaptive smoothing from the anisotropic diffusion with the perspective of an energy flow, providing new insights into application-specific filtering algorithm design. A symmetric energy flow of the anisotropic diffusion implies that the diffusion process conserves the total energy of an initial image. Thus, the anisotropic diffusion should be differentiated from the adaptive smoothing although they show similar behavior. For instance, Gilboa and Osher [14] proposed a non-local diffusion filter (PDE based smoothing) which is a corresponding counterpart of the non-local filter (kernel based smoothing) [12]. They showed that the proposed diffusion filter is superior to the conventional non-local filter in some applications such as image denoising and supervised image segmentation, since the symmetric energy flow does not tend to blur rare and singular regions [14]. Recently, Aubry *et al.* proposed a variant of the bilateral filter in which the normalization is removed [27]. This unnormalized version has a weaker effect when the sum of weights become smaller, which leads to generating slightly softer images, thus preventing halos at strong edges. Second, the behavior of a weighted average filter can be analyzed with the viewpoint of a PDE, since the normalization term used in the weighted average filter comes from the 'source' or 'sink' in the generalized continuity equation. Third, a new filter can be designed by properly modeling the 'source' or 'sink' in the proposed PDE according to specific applications. One feasible example is the RAD which is more robust against various outliers such as salt-and-pepper noise, Gaussian noise, and their mixture [28]. In this paper, as an extension of the RAD, the RCED is examined as well.

The paper is organized as follows: Section II briefly summarizes the adaptive smoothing and the anisotropic diffusion followed by traditional relationship between them [8], [19], [22]. Then, the adaptive smoothing is derived from a second order PDE and its behavior is analyzed with the view point of a PDE in Section III. In Section IV, the RAD and the RCED are introduced from the proposed PDE. Finally, Section V

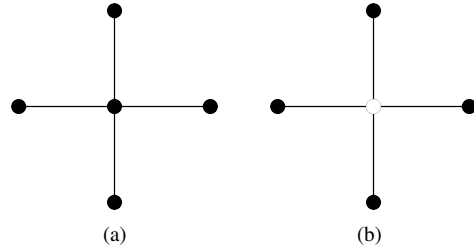


Fig. 1. Stencil diagram used in (a) the adaptive smoothing with \mathcal{N} , and (b) the anisotropic diffusion with 4-neighborhood \mathcal{N}_4 . White circles and black circles denote the center node \mathbf{p} and its neighborhood \mathbf{q} , respectively. Note that \mathcal{N} includes the center node as well.

concludes the paper with a discussion.

II. ADAPTIVE SMOOTHING AND ANISOTROPIC DIFFUSION

A. Adaptive Smoothing

The adaptive smoothing aims to regularize an image while preserving features. The image is repeatedly convolved with a kernel weighted by a measure of the discontinuity [8]. Let $I^{(t)}(\mathbf{p})$ denote an intensity value of $\mathbf{p} = (x, y)$ at the t^{th} iteration. A signal, filtered by the adaptive smoothing, is defined as follows.

$$I^{(t+1)}(\mathbf{p}) = \frac{1}{\chi^{(t)}(\mathbf{p})} \sum_{\mathbf{q} \in \mathcal{N}} I^{(t)}(\mathbf{q}) g_s(d^{(t)}(\mathbf{q}, \mathbf{p})) \quad (1)$$

with

$$\chi^{(t)}(\mathbf{p}) = \sum_{\mathbf{q} \in \mathcal{N}} g_s(d^{(t)}(\mathbf{q}, \mathbf{p})), \quad (2)$$

where $g_s(d^{(t)}(\mathbf{q}, \mathbf{p}))$ is a monotonically decreasing function according to the distance $d^{(t)}(\mathbf{q}, \mathbf{p}) = |I^{(t)}(\mathbf{q}) - I^{(t)}(\mathbf{p})|$ which discriminates the relative importance between points. \mathcal{N} is the set of neighboring pixels to the center node \mathbf{p} as shown in Fig. 1(a). Note that the center node is also included in \mathcal{N} .

B. Anisotropic Diffusion

The heat equation, or the diffusion, is a fundamental PDE that models the distribution of heat or temperature on a given domain over time. Perona and Malik applied this physics model to image processing, especially for edge preserving smoothing, with scale space theory [4]. They introduced a time and spatially varying diffusivity function into the diffusion model, which results in the anisotropic diffusion, as follows:

$$\partial_t I(\mathbf{p}) = \nabla \cdot [c^{(t)}(\mathbf{p}) \nabla I^{(t)}(\mathbf{p})], \quad (3)$$

where t denotes the time. ∇ and $\nabla \cdot$ denote the gradient and divergence operator, respectively. $c^{(t)}(\mathbf{p})$ defined as in (4) is a thermal diffusivity function satisfying $g_d(x) \rightarrow 0$ as $x \rightarrow \infty$.

$$c^{(t)}(\mathbf{p}) = g_d(\|\nabla I^{(t)}(\mathbf{p})\|) \quad (4)$$

The 1-D counterpart of the anisotropic diffusion as in (3) is discretized by an explicit finite difference method (FDM) as follows [29].

$$\begin{aligned} \partial_t I(x) &= \partial_x [c^{(t)}(x) \partial_x I^{(t)}(x)] \\ &\approx \frac{1}{2} \left(c^{(t)}(x-1) + c^{(t)}(x) \right) \left(I^{(t)}(x-1) - I^{(t)}(x) \right) \\ &\quad + \frac{1}{2} \left(c^{(t)}(x+1) + c^{(t)}(x) \right) \left(I^{(t)}(x+1) - I^{(t)}(x) \right), \quad (5) \end{aligned}$$

where

$$\begin{aligned} & \frac{1}{2} \left(c^{(t)}(x-1) + c^{(t)}(x) \right) \\ & \approx \frac{1}{2} \left[\begin{aligned} & g_d(|I^{(t)}(x-1) - I^{(t)}(x)|) \\ & + g_d(|I^{(t)}(x-1) - I^{(t)}(x)|) \end{aligned} \right] \\ & = g_d(|I^{(t)}(x-1) - I^{(t)}(x)|), \\ & \frac{1}{2} \left(c^{(t)}(x+1) + c^{(t)}(x) \right) \\ & \approx \frac{1}{2} \left[\begin{aligned} & g_d(|I^{(t)}(x+1) - I^{(t)}(x)|) \\ & + g_d(|I^{(t)}(x+1) - I^{(t)}(x)|) \end{aligned} \right] \\ & = g_d(|I^{(t)}(x+1) - I^{(t)}(x)|). \end{aligned} \quad (6)$$

Note that the first and second terms are approximated by the backward and forward differences, respectively [30]. Then, the 1D anisotropic diffusion is discretized by an explicit FDM with a forward Euler approximation as follows.

$$\begin{aligned} & [I^{(t+1)}(x) - I^{(t)}(x)]/\tau = \\ & = g_d(|I^{(t)}(x+1) - I^{(t)}(x)|)[I^{(t)}(x-1) - I^{(t)}(x)] \\ & + g_d(|I^{(t)}(x+1) - I^{(t)}(x)|)[I^{(t)}(x+1) - I^{(t)}(x)], \end{aligned} \quad (7)$$

where τ is an evolution step size.

Similarly, the 2D anisotropic diffusion as in (3) is discretized as follows.

$$\begin{aligned} & I^{(t+1)}(\mathbf{p}) = I^{(t)}(\mathbf{p}) \\ & + \tau \sum_{\mathbf{q} \in \mathcal{N}_4} g_d(|I^{(t)}(\mathbf{q}) - I^{(t)}(\mathbf{p})|)(I^{(t)}(\mathbf{q}) - I^{(t)}(\mathbf{p})) \end{aligned} \quad (8)$$

where \mathcal{N}_4 represents the 4-neighborhood of the center node \mathbf{p} , as shown in Fig. 1(b).

C. Traditional Relationship between Adaptive Smoothing and Anisotropic Diffusion

We review the traditional relationship between the adaptive smoothing and the anisotropic diffusion. We assume that, without loss of generality, the functions $g_s(\cdot)$ in (1) and $g_d(\cdot)$ in (4) is identical in that they play the same role, i.e., preventing the diffusion across different features. From here on, we hence denote these functions as $g(\cdot)$. The general relationship between two functions $c^{(t)}(\cdot)$ and $d^{(t)}(\cdot)$ can then be derived as follows.

$$\begin{aligned} & \frac{1}{2} \left(c^{(t)}(\mathbf{q}) + c^{(t)}(\mathbf{p}) \right) \\ & \approx g(|I^{(t)}(\mathbf{q}) - I^{(t)}(\mathbf{p})|) = g(d^{(t)}(\mathbf{q}, \mathbf{p})) \end{aligned} \quad (9)$$

Saint-Marc *et al.* formulated the 1-D case of the adaptive smoothing in (1) as follows [8].

$$\begin{aligned} & I^{(t+1)}(x) = c^{(t)}(x-1)I^{(t)}(x-1) \\ & + c^{(t)}(x)I^{(t)}(x) + c^{(t)}(x+1)I^{(t)}(x+1) \end{aligned} \quad (10)$$

with

$$c^{(t)}(x-1) + c^{(t)}(x) + c^{(t)}(x+1) = 1. \quad (11)$$

After plugging (11) into (10) and rearranging the equation, the following equation can be derived:

$$\begin{aligned} & I^{(t+1)}(x) - I^{(t)}(x) \\ & = c^{(t)}(x-1)[I^{(t)}(x-1) - I^{(t)}(x)] \\ & + c^{(t)}(x+1)[I^{(t)}(x+1) - I^{(t)}(x)] \end{aligned} \quad (12)$$

It is similar to the 1-D discrete implementation of the anisotropic diffusion in (7). Later, Barash showed that this is an inconsistent approximation of anisotropic diffusion in (7), since an extra term remains when the terms $c^{(t)}(x+1)$, $c^{(t)}(x-1)$ and $I^{(t)}(x+1)$, $I^{(t)}(x-1)$ are expanded with respect to $c^{(t)}(x)$ and $I^{(t)}(x)$, respectively, by using a Taylor series [19]. (See for more details in appendix of [19].) In order to address the inconsistency problem, Barash re-formulated the 1-D adaptive smoothing of (1) as follows [19]:

$$\begin{aligned} & I^{(t+1)}(x) = \frac{c^{(t)}(x-1)I^{(t)}(x-1) + c^{(t)}(x)I^{(t)}(x-1)}{2} \\ & + \frac{c^{(t)}(x)I^{(t)}(x)}{2} \\ & + \frac{c^{(t)}(x+1)I^{(t)}(x+1) + c^{(t)}(x)I^{(t)}(x+1)}{2}, \end{aligned} \quad (13)$$

with

$$\frac{c^{(t)}(x-1) + c^{(t)}(x)}{2} + c^{(t)}(x) + \frac{c^{(t)}(x+1) + c^{(t)}(x)}{2} = 1. \quad (14)$$

That is,

$$\begin{aligned} & g(|I^{(t)}(x-1) - I^{(t)}(x)|) + g(0) \\ & + g(|I^{(t)}(x+1) - I^{(t)}(x)|) = \chi^{(t)}(x) = 1. \end{aligned} \quad (15)$$

After similar manipulation to (12), we can derive the following equation:

$$\begin{aligned} & I^{(t+1)}(x) - I^{(t)}(x) = \\ & \frac{c^{(t)}(x-1) + c^{(t)}(x)}{2} [I^{(t)}(x-1) - I^{(t)}(x)] \\ & + \frac{c^{(t)}(x+1) + c^{(t)}(x)}{2} [I^{(t)}(x+1) - I^{(t)}(x)]. \end{aligned} \quad (16)$$

Obviously, (16) can be referred to as the 1-D discrete implementation of the anisotropic diffusion as in (7) [19]. However, this result is validated only when (14) or (15) is satisfied, i.e., the sum of weights is equal to 1, since the normalization used in the adaptive smoothing of (1) is not considered in (13), which will be explained in the next section.

III. DERIVATION OF ADAPTIVE SMOOTHING FROM A SECOND ORDER PDE

A. Problem Statement

In this section, we show that the adaptive smoothing is not equivalent to the anisotropic diffusion by exploring the characteristics of two approaches with the perspective of a normalization, an evolution step size, and an energy flow.

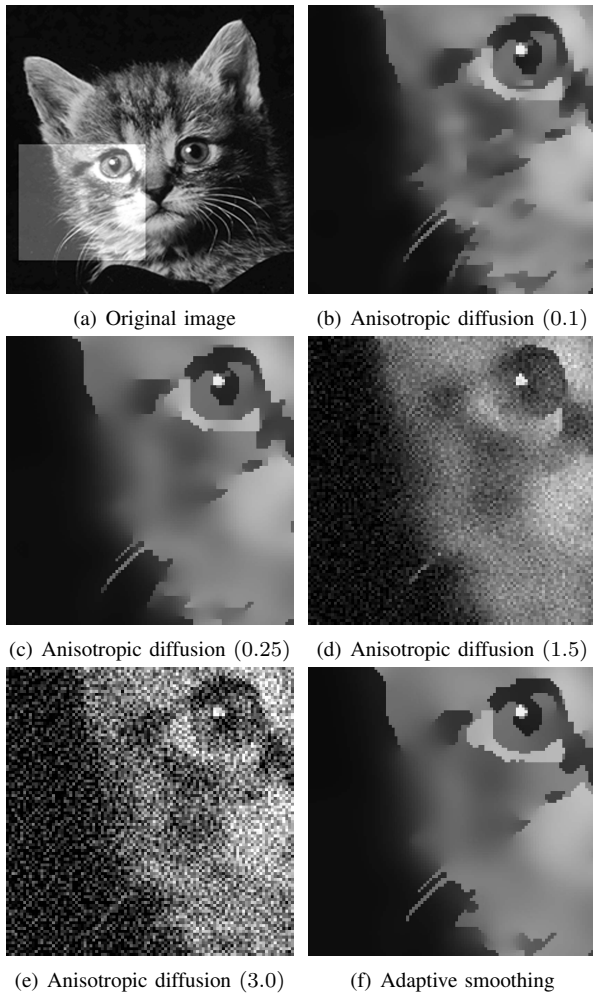


Fig. 2. Comparison of the anisotropic diffusion and the adaptive smoothing: (a) An original ‘cat’ image [10], the anisotropic diffusion when the evolution step size is set to (b) 0.10, (c) 0.25, (d) 1.50, and (e) 3.0, (f) the adaptive smoothing. The number of iteration is fixed to 50 in both anisotropic diffusion and adaptive smoothing. Gaussian kernel with an amplitude 1 and a fixed standard deviation 0.01, is used as $g(\cdot)$ in both methods. Note that the result of the anisotropic diffusion diverges when the evolution step size is larger than 0.25, i.e., the filtered results become noisy when the evolution step size is set to 1.5 or 3.0. Please see the electronic version for better visibility.

1) *Normalization*: The metric $d^{(t)}(\mathbf{q}, \mathbf{p})$ in (1) is generally defined by an intensity similarity between two pixels, and meets following conditions.

$$d^{(t)}(\mathbf{q}, \mathbf{p}) \geq 0 \quad (\text{non - negativity}) \quad (17)$$

$$d^{(t)}(\mathbf{q}, \mathbf{p}) = 0 \quad \text{if and only if } \mathbf{q} = \mathbf{p} \quad (\text{identity}) \quad (18)$$

$$d^{(t)}(\mathbf{q}, \mathbf{p}) = d^{(t)}(\mathbf{p}, \mathbf{q}) \quad (\text{symmetry}) \quad (19)$$

$$d^{(t)}(\mathbf{q}, \mathbf{p}) \leq d^{(t)}(\mathbf{q}, \mathbf{r}) + d^{(t)}(\mathbf{r}, \mathbf{p}) \quad (\text{triangle inequality}) \quad (20)$$

Since the weight function $g(d^{(t)}(\mathbf{q}, \mathbf{p}))$ is calculated by the distance metric $d^{(t)}(\mathbf{q}, \mathbf{p})$ whose value is always positive, the sum of weights in (14) or (15) is spatially varying according to the characteristics of the distance metric $d^{(t)}(\mathbf{q}, \mathbf{p})$, *not being fixed to 1*.

Proposition 1: The adaptive smoothing is equivalent to the anisotropic diffusion only when the sum of weights χ is equal to 1.

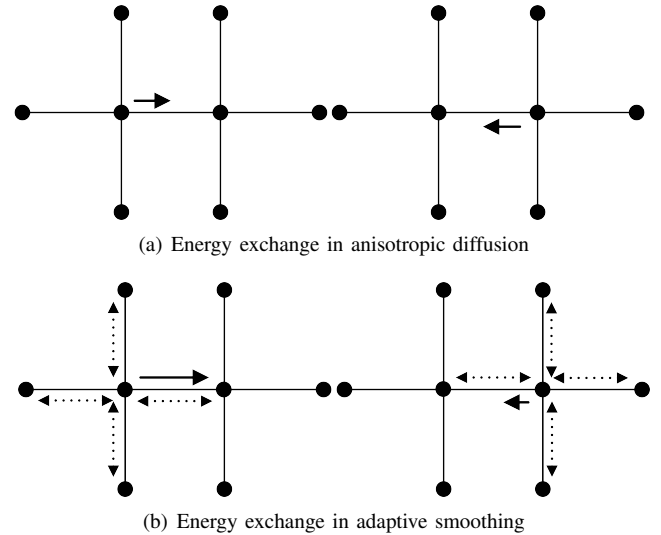


Fig. 3. Energy flow diagram: (a) An energy exchange between pixels adjoined is symmetry in the anisotropic diffusion. (b) In contrast to the anisotropic diffusion, the energy exchange is asymmetric in the adaptive smoothing due to the normalization. Solid-arrows indicate the energy flow in a corresponding direction, which is influenced by the dotted-arrows. The dotted-arrows indicate the influence of normalization.

Proof: Let us consider the following case.

$$\frac{c^{(t)}(x-1) + c^{(t)}(x)}{2} + c^{(t)}(x) + \frac{c^{(t)}(x+1) + c^{(t)}(x)}{2} = \chi^{(t)}(x), \quad (21)$$

where $\chi^{(t)}(x)$ is a normalization factor, and is an arbitrary constant that satisfies $\chi^{(t)}(x) > 0$.

After the same manipulation as (16), the following equation is derived:

$$\begin{aligned} I^{(t+1)}(x) - I^{(t)}(x) &= \\ &= \frac{c^{(t)}(x-1) + c^{(t)}(x)}{2} [I^{(t)}(x-1) - I^{(t)}(x)] \\ &+ \frac{c^{(t)}(x+1) + c^{(t)}(x)}{2} [I^{(t)}(x+1) - I^{(t)}(x)] \\ &+ (\chi^{(t)}(x) - 1)I^{(t)}(x), \end{aligned} \quad (22)$$

Thus, the adaptive smoothing is equivalent to the anisotropic diffusion only when the sum of weights $\chi^{(t)}(x)$ is equal to 1. ■

2) *Evolution Step Size*: It is assumed that the evolution step size of the anisotropic diffusion in (16) is 1, making it unstable. In general, when 1-D anisotropic diffusion is discretized by an explicit FDM, the evolution step size should be smaller than 0.5 (0.25 in 2-D case) in order to ensure its numerical stability [31]. Fig. 2 shows images filtered by (b)-(e) the anisotropic diffusion where the evolution step size varies from 0.10 to 3.0, and (f) the adaptive smoothing, respectively. We found that the result diverges, when the evolution step size of the anisotropic diffusion is larger than 0.25, i.e., the filtered results become noisy when the evolution step size is set to 1.5 or 3.0.

Recently, it was shown that each iteration of the adaptive smoothing can be referred to as one step of the anisotropic diffusion [23]. This relationship, however, still shares the same problems as described above, i.e., the anisotropic diffusion

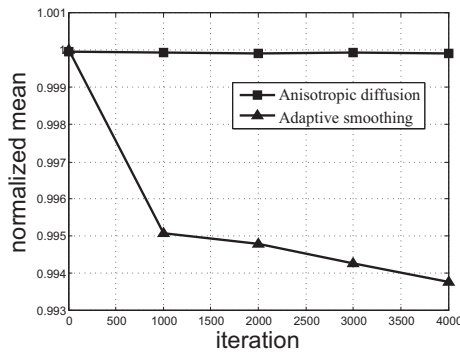


Fig. 4. Normalized mean value of the results filtered by the anisotropic diffusion and the adaptive smoothing according to the iteration with an initial condition as in Fig. 2(a). Gaussian kernel with an amplitude 1 and a fixed variance 0.01 is used as $g(\cdot)$ in both methods. It should be noted that the mean value of the image filtered by the anisotropic diffusion is preserved thanks to its symmetric energy flow.

derived from the adaptive smoothing in [23] is unstable since the evolution step size of the anisotropic diffusion is assumed to become 1.

3) *Energy Flow*: The energy of the anisotropic diffusion in (8) is exchanged in a symmetric manner, that is, the energy flow between two nodes \mathbf{p} and \mathbf{q} is determined by the center node itself, as shown in Fig. 3(a). In contrast, the energy of the adaptive smoothing is exchanged in an asymmetric manner due to the normalization [14], [32], and the energy flow is determined by their neighborhood nodes as well as the current node, as plotted by the dotted-arrows in Fig. 3(b). Fig. 4 shows the normalized mean value of the results filtered by the anisotropic diffusion and the adaptive smoothing according to iteration with an initial condition as in Fig. 2(a). The anisotropic diffusion preserves the mean of an initial image regardless of time, whereas the adaptive smoothing does not. However, (16) derived by Barash [19] does not reflect the asymmetric energy flow of the adaptive smoothing, i.e., the flow of (16) is always symmetric although it is derived from the adaptive smoothing, leading to the conclusion that the equivalence between the adaptive smoothing and the anisotropic diffusion is not valid.

B. Derivation of Adaptive Smoothing From a Second Order PDE

In this section, we first examine the origin of the anisotropic diffusion, and re-derive the adaptive smoothing from a second order PDE, considering the asymmetric energy flow.

The anisotropic diffusion is derived via the coupling of Fick's law with the continuity equation. Fick's law states that a concentration gradient causes a diffusion flux that aims to compensate for this concentration field as follows [33]:

$$J(\mathbf{p}) = -c^{(t)}(\mathbf{p})\nabla I(\mathbf{p}). \quad (23)$$

The generalized continuity equation is then expressed by:

$$\partial_t I(\mathbf{p}) = -\nabla \cdot J(\mathbf{p}) + s, \quad (24)$$

where s is a function that describes the generation or removal of I , so-called 'source' or 'sink'. Plugging Fick's law into the general continuity equation and setting s to 0, we derive

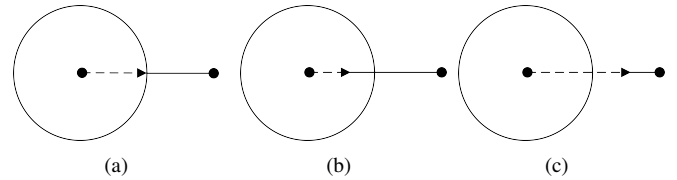


Fig. 5. Three cases of an energy flow in the adaptive smoothing. (a) the energy flow of the adaptive smoothing is exactly the same as that of the anisotropic diffusion. In case of (b) and (c), the energy flow of the adaptive smoothing is smaller, and larger than that of the anisotropic diffusion, respectively.

the anisotropic diffusion as in (3). The anisotropic diffusion is hence adiabatic as shown in Fig. 4 since the 'source' or 'sink' in the continuity equation is eliminated, making the energy flow symmetric, as shown in Fig. 3(a).

As mentioned in previous section, the energy flow in the adaptive smoothing is asymmetric, which enables us to classify the energy flow in the adaptive smoothing into three cases as shown in Fig. 5.

- First, the energy flow of the adaptive smoothing is exactly the same as that of the anisotropic diffusion as shown in Fig. 5(a), so there is no additional flow in the adaptive smoothing.
- Second, the energy flow of the adaptive smoothing can be smaller or larger than that of the anisotropic diffusion as shown in Fig. 5(b) and (c), corresponding that the sum of weights χ in (1) is larger or smaller than 1, respectively. It also implies that an additional flow exists in the adaptive smoothing. Specifically, \mathbf{p} in Fig. 5(b) and (c) can be considered as the 'sink' and 'source', respectively.

It leads to the conclusion that s in (24) exists in the adaptive smoothing as in (25).

$$\partial_t I(\mathbf{p}) = \nabla \cdot [c^{(t)}(\mathbf{p})\nabla I(\mathbf{p})] + s(\mathbf{p}), \quad (25)$$

where $s(\mathbf{p})$ is a spatially-varying function. It is worthy of noting that one can design a new filter by appropriately modeling $s(\mathbf{p})$ according to specific applications [28].

Then, *what function should be given as $s(\mathbf{p})$ in the adaptive smoothing?* By considering the energy flow in the adaptive smoothing as described in Fig. 5, $s(\mathbf{p})$ should meet the following criteria.

- First, it should scale the magnitude of the original flux $\nabla \cdot (c^{(t)}(\mathbf{p})\nabla I(\mathbf{p}))$ only while preserving its direction. It is worthy of noting that a rotation field can create an asymmetric flow as well, but it changes the direction/angle as well as the magnitude of a flow, which does not correspond to the adaptive smoothing.
- Second, its scaling strength depends on not only the current pixel but its neighboring pixels. When the current pixel is similar to the neighboring pixels, i.e., $\chi^{(t)}(\mathbf{p})$ is high, the flux decreases as shown in Fig. 5(b), corresponding that a scaling strength becomes smaller than 1 when the scaling strength is assumed to be 1 in case of Fig. 5(a), and *vice versa*. In summary, the scaling strength is inversely proportional to the sum of weights $\chi^{(t)}(\mathbf{p})$.

The following proposition can then be derived.

TABLE I
RELATION BETWEEN $s(\mathbf{p})$ AND $\kappa(\mathbf{p})$

	Fig.5(a)	Fig.5(b)	Fig.5(c)
\mathbf{p}	–	sink	source
$\chi^{(t)}(\mathbf{p})$	1	> 1	$0 < \cdot < 1$
$\kappa(\mathbf{p})$	1	$0 < \cdot < 1$	> 1
$s(\mathbf{p})$	0	< 0	> 0
$\ln[\kappa(\mathbf{p})]$	0	< 0	> 0
Anisotropic diffusion	0	–	–
Adaptive smoothing	0	0	0

Proposition 2: In the adaptive smoothing, $s(\mathbf{p})$ is a function of the original flux $\nabla \cdot [c^{(t)}(\mathbf{p})\nabla I(\mathbf{p})]$ and the sum of weights $\chi^{(t)}(\mathbf{p})$.

Proof: Equation (25) can be re-formulated by introducing a new function κ .

$$\partial_t I(\mathbf{p}) = \kappa(\mathbf{p})\nabla \cdot [c^{(t)}(\mathbf{p})\nabla I(\mathbf{p})] \quad (26)$$

where

$$\kappa(\mathbf{p}) = \frac{\nabla \cdot [c^{(t)}(\mathbf{p})\nabla I(\mathbf{p})] + s(\mathbf{p})}{\nabla \cdot [c^{(t)}(\mathbf{p})\nabla I(\mathbf{p})]}. \quad (27)$$

In the adaptive smoothing, the scaling strength of $\kappa(\mathbf{p})$ is equal to the reciprocal of the sum of weights $\chi^{(t)}(\mathbf{p})$ by the second criterion. By arranging (27) with respect to $s(\mathbf{p})$, the following equation is derived.

$$\begin{aligned} s(\mathbf{p}) &= (\kappa(\mathbf{p}) - 1) \nabla \cdot [c^{(t)}(\mathbf{p})\nabla I(\mathbf{p})] \\ &= \left(\frac{1}{\chi^{(t)}(\mathbf{p})} - 1 \right) \nabla \cdot [c^{(t)}(\mathbf{p})\nabla I(\mathbf{p})] \end{aligned} \quad (28)$$

It is worth noting that the scaling factor $\kappa(\mathbf{p})$ in (26) is always larger than 0 since it should adjust the magnitude of flux only as in the first criterion.

Corollary 1: $\kappa(\mathbf{p})$ is a ‘source’ or ‘sink’ in the log diffusion equation.

Proof: Since $\kappa(\mathbf{p}) > 0$, without loss of generality, we analyze (26) in the log domain by assuming that it becomes an equilibrium state as time t goes infinite.

$$\ln[\partial_t I(\mathbf{p})] = \ln \left[\nabla \cdot [c^{(t)}(\mathbf{p})\nabla I(\mathbf{p})] \right] + \ln[\kappa(\mathbf{p})] \quad (29)$$

By comparing (29) with (25), one can notice that (29) is the anisotropic diffusion in the log domain. $\ln[\kappa(\mathbf{p})]$ is hence called the ‘source’ or ‘sink’ in the log diffusion equation, which can be defined by

$$\ln[\kappa(\mathbf{p})] = \ln \left[1 + \frac{s(\mathbf{p})}{\nabla \cdot [c^{(t)}(\mathbf{p})\nabla I(\mathbf{p})]} \right]. \quad (30)$$

When $s(\mathbf{p})$ becomes 0 as in Fig. 5(a), i.e., \mathbf{p} is neither a ‘source’ nor ‘sink’, it corresponds $\ln[\kappa(\mathbf{p})]$ is 0. In contrast, when \mathbf{p} is a ‘sink’ ($s(\mathbf{p}) < 0$) in Fig. 5(b) or a ‘source’ ($s(\mathbf{p}) > 0$) in Fig. 5(c), it corresponds to $\ln[\kappa(\mathbf{p})] < 0$ or $\ln[\kappa(\mathbf{p})] > 0$, respectively. Table I summarizes three cases of Fig. 5. ■

Equation (26) is then re-written by incorporating $\chi^{(t)}(\mathbf{p})$, which leads to the second order PDE as follows:

$$\chi^{(t)}(\mathbf{p})\partial_t I(\mathbf{p}) = \nabla \cdot [c^{(t)}(\mathbf{p})\nabla I(\mathbf{p})]. \quad (31)$$

Note that when $\chi^{(t)}(\mathbf{p})$ is set to 1, i.e. $s(\mathbf{p}) = 0$, as in Fig. 5(a), the adaptive smoothing in (31) becomes the anisotropic diffusion in (3), and this exactly coincides with the constraint (14) or (15), i.e., sum of weights becomes 1. Therefore, the proposition 1 is supported once more.

Equation (31) is then discretized by an explicit FDM with a forward Euler approximation as follows.

$$\begin{aligned} I^{(t+1)}(\mathbf{p}) &= I^{(t)}(\mathbf{p}) \\ &+ \tau \frac{\sum_{\mathbf{q} \in \mathcal{N}_4} g(|I^{(t)}(\mathbf{q}) - I^{(t)}(\mathbf{p})|) (I^{(t)}(\mathbf{q}) - I^{(t)}(\mathbf{p}))}{g(0) + \sum_{\mathbf{q} \in \mathcal{N}_4} g(|I^{(t)}(\mathbf{q}) - I^{(t)}(\mathbf{p})|)} \end{aligned} \quad (32)$$

Proposition 3: The adaptive smoothing in (1) is equivalent to (32) when the evolution step size τ is 1.

Proof: Let us re-formulate the 1-D case of the adaptive smoothing in (1) in order to link it with the second order PDE, considering the sum of weights χ . Note that the normalization is considered in (33), different from (13).

$$I^{(t+1)}(x) = \alpha I^{(t)}(x-1) + \beta I^{(t)}(x) + \gamma I^{(t)}(x+1), \quad (33)$$

where

$$\alpha = \left(\frac{c^{(t)}(x-1) + c^{(t)}(x)}{2} \right) / \chi^{(t)}(x),$$

$$\beta = c^{(t)}(x) / \chi^{(t)}(x), \quad (34)$$

$$\gamma = \left(\frac{c^{(t)}(x+1) + c^{(t)}(x)}{2} \right) / \chi^{(t)}(x).$$

where

$$\begin{aligned} \frac{c^{(t)}(x-1) + c^{(t)}(x)}{2} + c^{(t)}(x) \\ + \frac{c^{(t)}(x+1) + c^{(t)}(x)}{2} = \chi^{(t)}(x). \end{aligned} \quad (35)$$

Note that α , β , and γ are derived by using (6). In contrast to (22), the following equation is always satisfied regardless of $\chi^{(t)}(x)$ since the normalization is embedded in α , β , and γ :

$$\alpha + \beta + \gamma = 1. \quad (36)$$

By substituting α , β , and γ in (33) with (34), we derive the

following equation:

$$\begin{aligned}
& I^{(t+1)}(x) - I^{(t)}(x) \\
&= \left(\frac{c^{(t)}(x-1) + c^{(t)}(x)}{2\chi^{(t)}(x)} \right) (I^{(t)}(x-1) - I^{(t)}(x)) \\
&+ \left(\frac{c^{(t)}(x+1) + c^{(t)}(x)}{2\chi^{(t)}(x)} \right) (I^{(t)}(x+1) - I^{(t)}(x)) \\
&= \frac{g(|I^{(t)}(x-1) - I^{(t)}(x)|)}{\left[\frac{g(|I^{(t)}(x-1) - I^{(t)}(x)|)}{+g(0) + g(|I^{(t)}(x+1) - I^{(t)}(x)|)} \right]} \\
&\cdot (I^{(t)}(x-1) - I^{(t)}(x)) \\
&+ \frac{g(|I^{(t)}(x+1) - I^{(t)}(x)|)}{\left[\frac{g(|I^{(t)}(x-1) - I^{(t)}(x)|)}{+g(0) + g(|I^{(t)}(x+1) - I^{(t)}(x)|)} \right]} \\
&\cdot (I^{(t)}(x+1) - I^{(t)}(x)). \tag{37}
\end{aligned}$$

This represents the implementation of a second order PDE in (32) with the evolution step size τ being 1, meaning that the adaptive smoothing in (33) is linked with the second order PDE with the ‘source’ or ‘sink’.

Remark 1: The normalization term of a weighted average filter such as the adaptive smoothing [8] generates an asymmetric energy flow, and comes from the generalized continuity equation in which the ‘source’ or ‘sink’ exists.

Corollary 2: All \mathbf{p} 's in the adaptive smoothing are ‘sink’ if $g(0) = 1$.

Proof: If $g(0) = 1$, $\kappa(\mathbf{p})$ is always smaller than 1 as in Fig. 5(b), which makes $\ln[\kappa(\mathbf{p})] < 0$ ($s(\mathbf{p}) < 0$).

Therefore, as shown in Fig. 4, the normalized mean value of the results filtered by the adaptive smoothing, where $g(0)$ is set to 1, monotonically decreases.

C. The Behavior of Adaptive Smoothing

In this section, we will examine the behavior of the adaptive smoothing such as the maximum principle and stability condition within the framework of a PDE.

1) *The Maximum Principle:* We verify that (32), which was proven to be equivalent to the adaptive smoothing, satisfies the maximum principle, i.e., no new maxima and minima appear as an image is filtered. Although the anisotropic diffusion in (8) also satisfies the maximum principle [4], the anisotropic diffusion and the adaptive smoothing have a different theoretical origin, as mentioned in section III-B.

Proposition 4: The adaptive smoothing satisfies the maximum principle.

Proof: When the 4-neighborhood is used, the maximum and minimum values among the center node \mathbf{p} and \mathcal{N}_4 are defined by

$$M^{(t)}(\mathbf{p}) = \max \left\{ I^{(t)}(\mathbf{p}), I^{(t)}(\mathbf{q}) \Big|_{\mathbf{q} \in \mathcal{N}_4} \right\}, \tag{38}$$

$$m^{(t)}(\mathbf{p}) = \min \left\{ I^{(t)}(\mathbf{p}), I^{(t)}(\mathbf{q}) \Big|_{\mathbf{q} \in \mathcal{N}_4} \right\}. \tag{39}$$

Equation (32) can be modified as:

$$\begin{aligned}
& I^{(t+1)}(\mathbf{p}) \\
&= I^{(t)}(\mathbf{p}) \left(1 - \tau \frac{\sum_{\mathbf{q} \in \mathcal{N}_4} g(|I^{(t)}(\mathbf{q}) - I^{(t)}(\mathbf{p})|)}{g(0) + \sum_{\mathbf{q} \in \mathcal{N}_4} g(|I^{(t)}(\mathbf{q}) - I^{(t)}(\mathbf{p})|)} \right) \\
&+ \tau \frac{\sum_{\mathbf{q} \in \mathcal{N}_4} g(|I^{(t)}(\mathbf{q}) - I^{(t)}(\mathbf{p})|) I^{(t)}(\mathbf{q})}{g(0) + \sum_{\mathbf{q} \in \mathcal{N}_4} g(|I^{(t)}(\mathbf{q}) - I^{(t)}(\mathbf{p})|)} \\
&\leq M^{(t)}(\mathbf{p}) \left(1 - \tau \frac{\sum_{\mathbf{q} \in \mathcal{N}_4} g(|I^{(t)}(\mathbf{q}) - I^{(t)}(\mathbf{p})|)}{g(0) + \sum_{\mathbf{q} \in \mathcal{N}_4} g(|I^{(t)}(\mathbf{q}) - I^{(t)}(\mathbf{p})|)} \right) \\
&+ \tau \frac{\sum_{\mathbf{q} \in \mathcal{N}_4} g(|I^{(t)}(\mathbf{q}) - I^{(t)}(\mathbf{p})|) M^{(t)}(\mathbf{p})}{g(0) + \sum_{\mathbf{q} \in \mathcal{N}_4} g(|I^{(t)}(\mathbf{q}) - I^{(t)}(\mathbf{p})|)} = M^{(t)}(\mathbf{p}). \tag{40}
\end{aligned}$$

Similarly,

$$\begin{aligned}
& I^{(t+1)}(\mathbf{p}) \\
&\geq m^{(t)}(\mathbf{p}) \left(1 - \tau \frac{\sum_{\mathbf{q} \in \mathcal{N}_4} g(|I^{(t)}(\mathbf{q}) - I^{(t)}(\mathbf{p})|)}{g(0) + \sum_{\mathbf{q} \in \mathcal{N}_4} g(|I^{(t)}(\mathbf{q}) - I^{(t)}(\mathbf{p})|)} \right) \\
&+ \tau \frac{\sum_{\mathbf{q} \in \mathcal{N}_4} g(|I^{(t)}(\mathbf{q}) - I^{(t)}(\mathbf{p})|) m^{(t)}(\mathbf{p})}{g(0) + \sum_{\mathbf{q} \in \mathcal{N}_4} g(|I^{(t)}(\mathbf{q}) - I^{(t)}(\mathbf{p})|)} = m^{(t)}(\mathbf{p}). \tag{41}
\end{aligned}$$

Thus,

$$m^{(t)}(\mathbf{p}) \leq I^{(t+1)}(\mathbf{p}) \leq M^{(t)}(\mathbf{p}). \tag{42}$$

2) *Stability:* It is somewhat intuitive that the normalization term prevents filtered images from diverging. It is related to the maximum norm stability in graph theory [17]. To the best of our knowledge, there have been no studies exploring this observation in the viewpoint of a PDE.

Proposition 5: The adaptive smoothing is always stable.

Proof: The stability condition of (32) is $0 \leq \tau \leq 5/4$, since the weight of the center node \mathbf{p} should be between 0 and 1 in order to ensure the stability as follows:

$$\begin{aligned}
& \tau < \max \left(\frac{g(0) + \sum_{\mathbf{q} \in \mathcal{N}_4} g(|I^{(t)}(\mathbf{q}) - I^{(t)}(\mathbf{p})|)}{\sum_{\mathbf{q} \in \mathcal{N}_4} g(|I^{(t)}(\mathbf{q}) - I^{(t)}(\mathbf{p})|)} \right) \\
&= \max \left(1 + \frac{g(0)}{\sum_{\mathbf{q} \in \mathcal{N}_4} g(|I^{(t)}(\mathbf{q}) - I^{(t)}(\mathbf{p})|)} \right) = 5/4. \tag{43}
\end{aligned}$$

We showed that the adaptive smoothing is a discrete approximation of (31) with the evolution step size being 1. Since the evolution step size in the adaptive smoothing is always smaller than 5/4 regardless of the function $g(\cdot)$, adaptive smoothing is always stable.

IV. INSTANTIATIONS OF THE PROPOSED PDE: ROBUST DIFFUSION

In this section, two specific diffusion methods are instantiated by leveraging the asymmetric energy flow in the diffusion. First, the RAD [28] is derived by differently modeling the ‘source’ or ‘sink’ in the proposed PDE. Based on this observation, the RCED is further proposed, which preserves universal features and enhances coherence structures better than the conventional one [34], [36], [37].

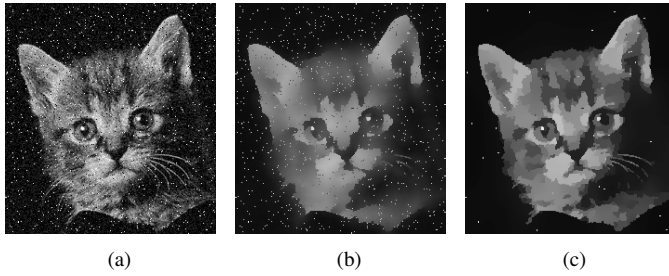


Fig. 6. An example of the anisotropic diffusion [4] and the RAD. (a) a degraded image, (b) the anisotropic diffusion, and (c) the RAD.

A. RAD

The RAD regularizes the image with an assumption that the adiabatic process such as the diffusion is not suitable in handling the outliers, e.g., impulsive noise [28]. Namely, an additional flux exists in the RAD so that the ‘source’ or ‘sink’ $s(\mathbf{p})$ in (25) is not 0, as opposed to the anisotropic diffusion [4]. The additional flux plays a role in such a way that the outlier signal is compensated by adaptively changing the amount of flux according to the local topology of the neighborhood, which results in reducing the influence of outliers significantly.

Ham *et al.* modeled $\kappa(\mathbf{p})$ as follows [28].

$$\kappa(\mathbf{p}) = \frac{1}{\chi^{(t)}(\mathbf{p}) - g(0)}. \quad (44)$$

The quantity of $\chi^{(t)}(\mathbf{p}) - g(0)$ is an indicator of the outlier, e.g., when this quantity is small, it implies that the center node is likely to be an outlier.

Then, the RAD is defined as follows.

$$[\chi^{(t)}(\mathbf{p}) - g(0)]\partial_t I(\mathbf{p}) = \nabla \cdot [c^{(t)}(\mathbf{p})\nabla I(\mathbf{p})]. \quad (45)$$

Note that the anisotropic diffusion [4] in (3), the adaptive smoothing [8] in (31) and the RAD in (45) are all the special case of the PDE of (26).

Fig. 6 shows an example of (b) the anisotropic diffusion [4] and (c) the RAD with (a) a degraded image. The initial ‘cat’ image [10] was degraded by the Gaussian noise with a standard deviation 0.1 and the impulsive noise with a density of 0.05. All parameters were set equal in both methods: $g(\cdot)$ as the Gaussian kernel with an amplitude 1 and a fixed standard deviation 0.01, an evolution step size τ of 0.25, and the number of iteration t of 500. It demonstrates that the RAD can handle the mixture noise very well, in contrast to the conventional anisotropic diffusion. Please refer to [28] for more results and intensive analysis of the RAD.

B. RCED

In this section, we further propose the RCED by incorporating additional fluxes into coherence enhancing diffusion in a similar manner to the RAD, making the proposed diffusion more robust against outliers as well as better enhance coherence structures.

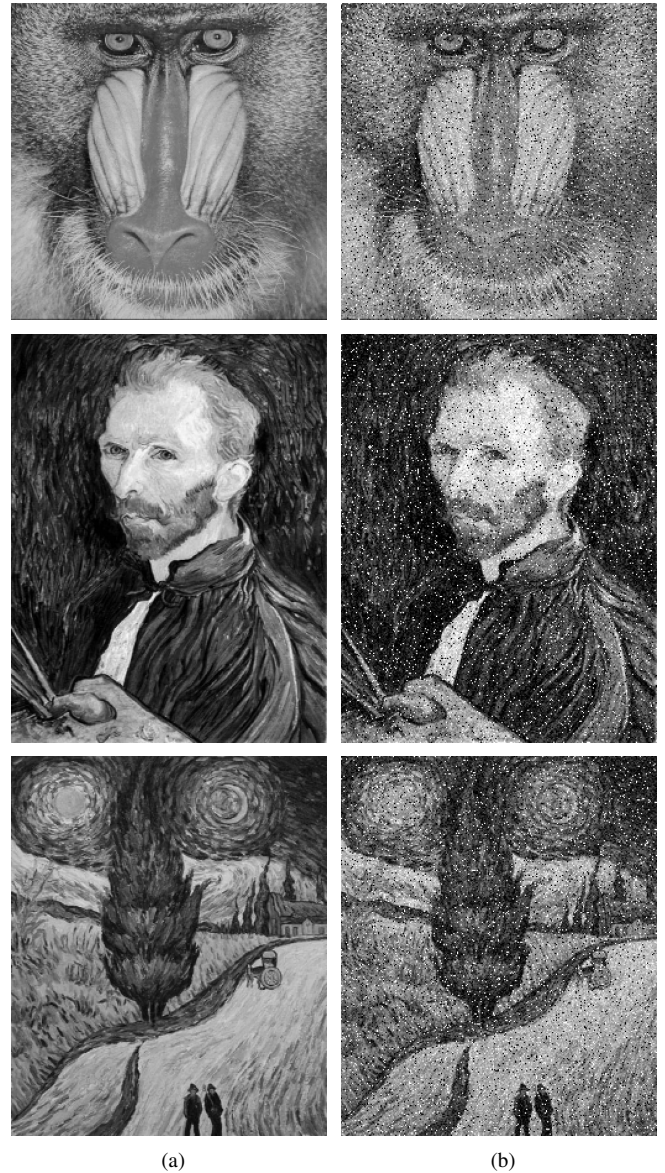


Fig. 7. Test sequences: (a) original images and (b) images corrupted by the Gaussian noise with a standard deviation of 0.1, and the impulsive noise with a density of 0.1.

1) *RCED*: Over the last two decades, there have been many studies on analyzing and enhancing the flow-like structure in the field of image processing [34], [35], [36], [37]. It has been usually done by a well-established tool from texture analysis based on the structure tensor (second moment matrix), the eigenvalues and eigenvectors of which provide us with all required information for speculating the structure embedded in the image [39].

First, let us define the structure tensor as follows:

$$\begin{aligned} \mathbf{J}_\rho &= K_\rho(\mathbf{p}) * \left[\nabla I_\sigma^{(t)}(\mathbf{p}) \nabla I_\sigma^{(t)}(\mathbf{p})^T \right] \\ &= \lambda_+ \theta_+ \theta_+^T + \lambda_- \theta_- \theta_-^T. \end{aligned} \quad (46)$$

where

$$K_\sigma(\mathbf{p}) = \frac{1}{2\pi\sigma^2} \exp\left(-\frac{\|\mathbf{p}\|^2}{2\sigma^2}\right), \quad (47)$$

$$\nabla I_\sigma^{(t)}(\mathbf{p}) = K_\sigma(\mathbf{p}) * \nabla I^{(t)}(\mathbf{p}). \quad (48)$$

This matrix is symmetric and positive definite, thus has two eigenvalues λ_+ , λ_- and corresponding eigenvectors θ_+ , θ_- which are tangential and orthogonal to $\nabla I_\sigma^{(t)}(\mathbf{p})$, respectively. The eigenvalues of $\mathbf{J}_\rho = \begin{pmatrix} j_{11} & j_{12} \\ j_{12} & j_{22} \end{pmatrix}$ are

$$\lambda_\pm = \frac{1}{2}(j_{11} + j_{22} \pm \Delta), \quad (49)$$

where

$$\Delta = \sqrt{(j_{11} - j_{22})^2 + 4j_{12}^2}. \quad (50)$$

Note that in a scalar image, the eigenvalues and eigenvectors of \mathbf{J}_0 are

$$\lambda_+ = \|\nabla I\|^2, \quad \lambda_- = 0 \quad (51)$$

and

$$\theta_+ = \frac{\nabla I}{\|\nabla I\|}, \quad \theta_- = \frac{\nabla I^\perp}{\|\nabla I\|}. \quad (52)$$

Directly employing the structure tensor \mathbf{J}_ρ as the diffusion tensor will lead to fast diffusion across the edge and slow diffusion along the edge, which is opposite to our intention [40]. For enhancing coherence within the flow-like structure, a regularization should act mainly along the flow direction. Also, the smoothing should increase according to the strength of its orientation which can be measured by some metric, e.g., $(\lambda_+ - \lambda_-)^2$ becomes large for strongly differing eigenvalues, and tends to zero for isotropic structures. Therefore, the diffusion tensor is constructed as in (53) with the same eigenvectors as the structure tensor \mathbf{J}_ρ [41], [42]:

$$\mathbf{D}^{(t)}(\mathbf{p}) = \lambda_1 \theta_+ \theta_+^T + \lambda_2 \theta_- \theta_-^T \quad (53)$$

The diffusion tensor $\mathbf{D}^{(t)}(\mathbf{p}) = \begin{pmatrix} d_{11} & d_{12} \\ d_{12} & d_{22} \end{pmatrix}$ is a 2×2 symmetric and positive definite matrix with two positive eigenvalues λ_1 , λ_2 and two corresponding eigenvectors θ_+ , θ_- . Each component can be calculated as follows.

$$\begin{aligned} d_{11} &= \frac{1}{2} \left[\lambda_1 + \lambda_2 - \frac{(\lambda_2 - \lambda_1)(j_{11} - j_{22})}{\Delta} \right], \\ d_{12} &= \frac{(\lambda_1 - \lambda_2)j_{12}}{\Delta}, \\ d_{22} &= \frac{1}{2} \left[\lambda_1 + \lambda_2 + \frac{(\lambda_2 - \lambda_1)(j_{11} - j_{22})}{\Delta} \right]. \end{aligned} \quad (54)$$

where the eigenvalues are

$$\begin{aligned} \lambda_1 &= \omega \\ \lambda_2 &= \begin{cases} \omega & \text{if } \lambda_+ = \lambda_- \\ \omega + (1 - \omega) \exp \left\{ -\frac{C}{(\lambda_+ - \lambda_-)^2} \right\} & \text{else} \end{cases} \end{aligned} \quad (55)$$

$\omega \in (0, 1)$ represents the regularization parameter which keeps the diffusion tensor positive definite [34]. $C > 0$ serves as a threshold parameter: $\lambda_2 \approx 1$ for $(\lambda_+ - \lambda_-)^2 \gg C$, and $\lambda_2 \approx \omega$ for $(\lambda_+ - \lambda_-)^2 \ll C$.

Then, the RCED is defined as follows:

$$\partial_t I(\mathbf{p}) = \kappa(\mathbf{p}) \nabla \cdot [\mathbf{D}^{(t)}(\mathbf{p}) \nabla I(\mathbf{p})]. \quad (56)$$

Similar to RAD, the ‘source’ or ‘sink’ in (56) is modeled as

$$\kappa(\mathbf{p}) = \frac{1}{\chi^{(t)}(\mathbf{p}) - g(0)}. \quad (57)$$

Note that $\kappa(\mathbf{p})$ is an isotropic since $\kappa(\mathbf{p})$ which is an indicator of the existence of the outliers, is irrelevant to an orientation of the edges. In other words, it is assumed that a probability of being corrupted by the outliers is independent of the orientation of the edges.

2) *Experimental Results*: To verify the performance, we compared the proposed method with the conventional coherence enhancing diffusion (CED) [34] and other related methods such as the anisotropic Kuwahara filter (AKF) [36] and the coherence enhancing shock filter (CES) [37]. These were applied to original images and images degraded by the mixture noises, i.e., the Gaussian noise with a standard deviation of 0.1 and the impulsive noise with a density of 0.1, as shown in Fig. 7. All the parameters were fixed during experiments. In the CED and the RCED, $\rho = 5$, $\sigma = 0.7$, $\omega = 0.01$ and $C = 0.001$. The number of iteration and the evolution step size were set to 100 and 0.2, respectively. The Gaussian kernel with a standard deviation 0.01 was used as $g(\cdot)$. In the AKF and the CES, the parameters were set to default values used in [36] and [37], respectively. Note that the filtering results of the two methods were produced by authors-provided softwares [38].

Fig. 8(a) shows that the Gaussian noise can be effectively handled by the CED [34], but impulsive noise still exists even after long evolution. Note that the vector ∇I_0 and the matrix \mathbf{J}_0 are regularized by the Gaussian kernel K in constructing the diffusion tensor so some outliers have been eliminated before the diffusion process. The AKF is the anisotropic counterpart of the weighted Kuwahara filter [43], thus artifacts which exist in the Kuwahara filter are avoided while directional image features are better preserved and emphasized. Fig. 8(b) shows that the AKF is robust against the outliers [36], but the region boundaries are distorted. The CES is not robust against the outliers, and even the outliers are sharpened and enhanced since the shock filter is embedded in the CES. In contrast, the RCED handles the impulsive noise as well as the Gaussian noise very well. Furthermore, it can preserve singular features better than other methods, e.g., mandrill’s eye.

The same experiments were conducted with the noise-free image as shown in Fig. 9. It also demonstrates the proposed method is more capable of enhancing the flow-like structures than other methods. Although the CED enhances the coherence structure well, it also blurs some important features. Meanwhile, the diffusion velocity of the proposed method automatically decreases when the features begin to be flattened, i.e., $[\chi^{(t)}(\mathbf{p}) - g(0)]$, an indicator of the existence of the outliers, increases, thus leading to preserving important features while enhancing the coherence structures. The CES sharpens and enhances the coherence structure well, but the additional procedure such as shock process is needed. We also found that the coherence enhancing capability of the RCED is better than that of the AKF (see mandrill’s fur).

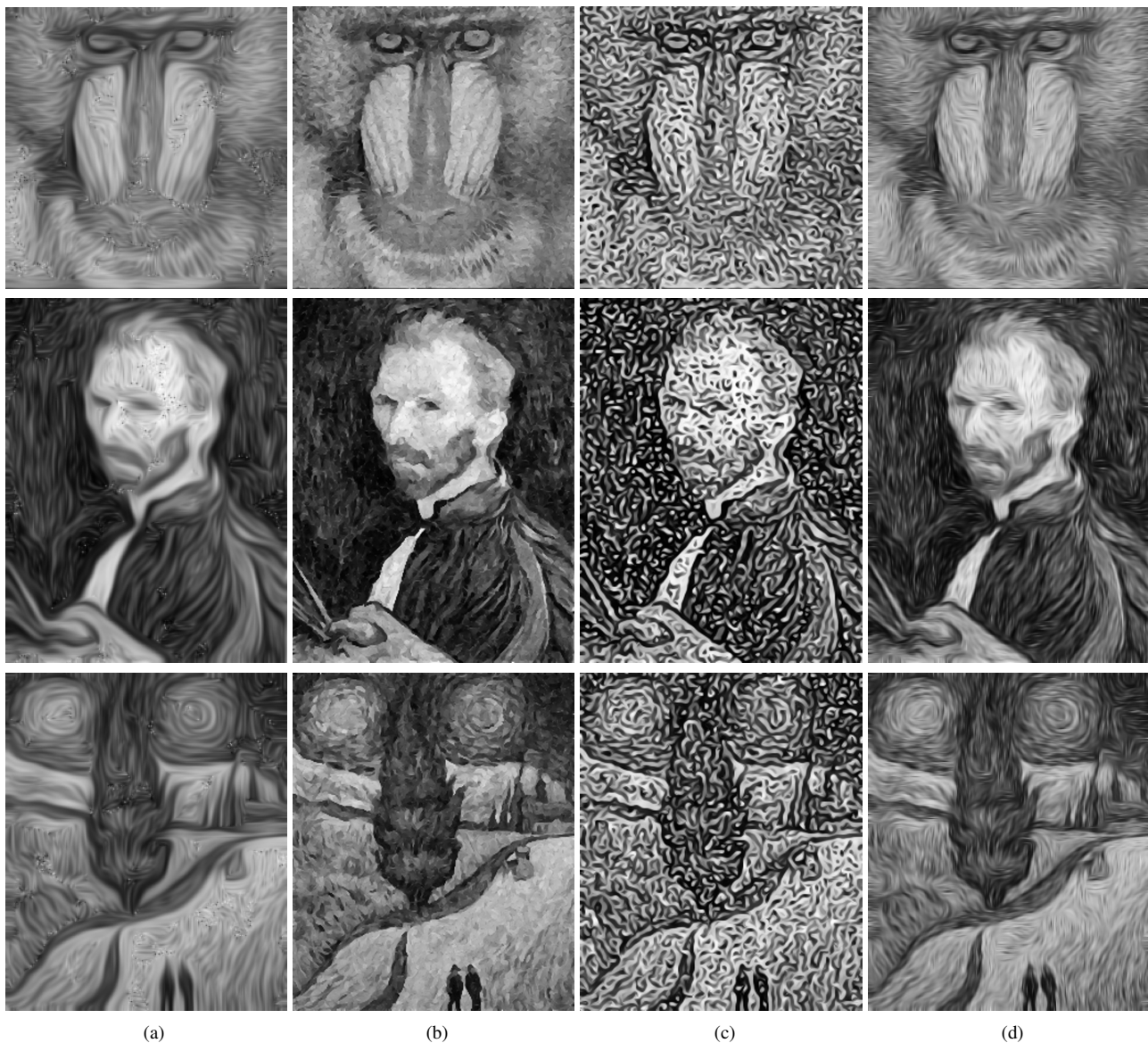


Fig. 8. Filtering results for corrupted images of Fig. 7(b): (a) the coherence enhancing diffusion (CED) [34], (b) the anisotropic Kuwahara filter (AKF) [36], (c) the coherence enhancing shock filter (CES) [37], and (d) the robust coherence enhancing diffusion (RCED). All parameters are fixed during experiments: In the CED and the RCED, $\rho = 5$, $\sigma = 0.7$, $\omega = 0.01$ and $C = 0.001$. The number of iteration and the evolution step size were set to 100 and 0.2, respectively. In the AKF and the CES, the parameters are set to default values used in [36] and [37], respectively. Note that the results of both methods were produced by using authors-provided softwares [38].

V. CONCLUSION

This paper differentiated the adaptive smoothing from the anisotropic diffusion in the viewpoint of a normalization, an evolution step size, and an energy flow. While the anisotropic diffusion has a symmetric flow since the diffusion is theoretically an adiabatic process, the adaptive smoothing has an asymmetric energy flow. Based on this principle, the adaptive smoothing was drawn from the generalized second order PDE where the ‘source’ or ‘sink’ exists. It provides new insights into application-specific filtering algorithm design such as the non-local diffusion [14] and the unnormalized bilateral filter [27]. Also, the behavior of the adaptive smoothing such as the maximum principle and stability has been examined with the perspective of a PDE by leveraging that the ‘source’ or ‘sink’ is closely related to the normalization term of the adaptive

smoothing. Furthermore, new diffusion filters such as the RAD and the RCED have been designed by properly modeling the ‘source’ or ‘sink’, thus generating the asymmetric diffusion flow which is more robust against the outliers.

REFERENCES

- [1] J-F. Aujol, G. Gilboa, T. Chan, and S. Osher, “Structure- Texture Image Decomposition - Modeling, Algorithms, and Parameter Selection,” *Int. J. Comput. Vis.*, vol. 67, no. 1, pp. 111-136, 2006.
- [2] K. Dabov, A. Foi, V. Katkovnik, and K. Egiazarian, “Image Denoising by Sparse 3-D Transform-Domain Collaborative Filtering,” *IEEE Trans. Image Process.*, vol. 16, no. 8, pp. 2080-2095, 2007.
- [3] J. Portilla, V. Strela, M. J. Wainwright, and E. P. Simoncelli, “Image Denoising Using Scale Mixtures of Gaussians in the Wavelet Domain,” *IEEE Trans. Image Process.*, vol. 12, no. 11, pp. 1338-1351, 2003.
- [4] P. Perona and J. Malik, “Scale-Space and Edge Detection Using Anisotropic Diffusion,” *IEEE Trans. Pattern Anal. Mach. Intell.*, vol. 12, no. 7, pp. 629-639, 1990.

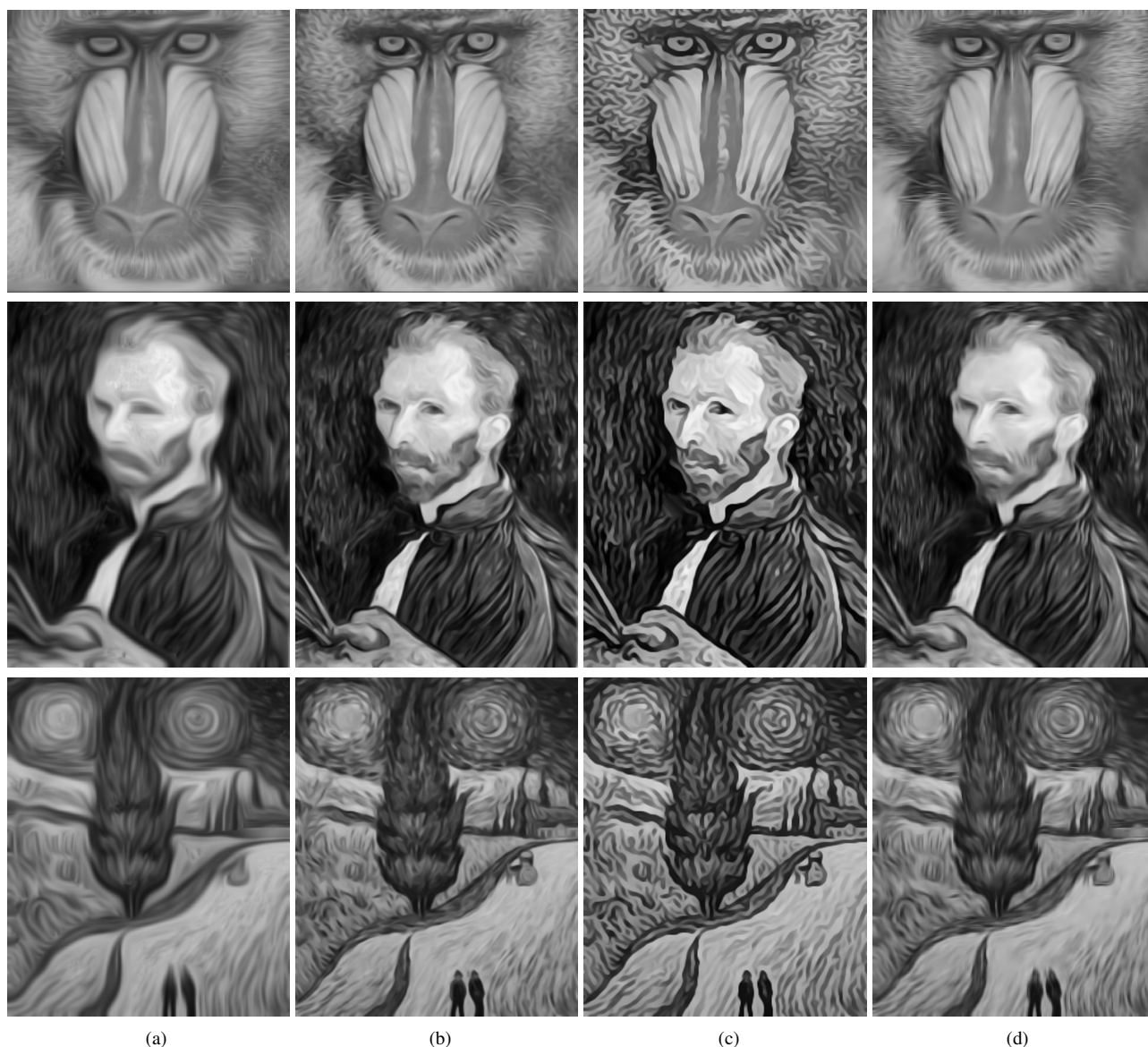


Fig. 9. Filtering results for original images of Fig. 7(a): (a) the coherence enhancing diffusion (CED) [34], (b) the anisotropic Kuwahara filter (AKF) [36], (c) the coherence enhancing shock filter (CES) [37], and (d) the robust coherence enhancing diffusion (RCED). All the parameters were set equal to Fig. 8.

- [5] A. Chambolle, "An Algorithm for Total Variation Minimization and Applications," *J. Math. Imaging Vision*, vol. 20, no. 1-2, pp. 89-97, 2004.
- [6] G. Steidl, J. Weickert, T. Brox, P. Mrazek and M. Welk, "On the Equivalence of Soft Wavelet Shrinkage, Total Variation Diffusion, Total Variation Regularization, and SIDES," *SIAM J. Numer. Anal.*, vol. 42, no. 2, pp. 686-713, 2005.
- [7] M. Welk, J. Weickert, and G. Steidl, "From Tensor-Driven Diffusion to Anisotropic Wavelet Shrinkage," in *Proc. Eur. Conf. Comput. Vis.*, pp. 391-403, 2006.
- [8] P. Saint-Marc, J. S. Chen, and G. Medioni, "Adaptive Smoothing: A General Tool for Early Vision," *IEEE Trans. Pattern Anal. Mach. Intell.*, vol. 13, no. 6, pp. 514-529, 1991.
- [9] A. Goshtasby and M. Satter, "An Adaptive Window Mechanism for Image Smoothing," *Comput. Vis. Image Underst.*, vol. 111, no. 2, pp. 155-169, 2008.
- [10] C. Tomasi and R. Manduchi, "Bilateral Filtering for Gray and Color Images," in *Proc. Int. Conf. Comput. Vis.*, pp. 839-846, 1998.
- [11] D. Comaniciu and P. Meer, "Mean Shift: A Robust Approach Toward Feature Space Analysis," *IEEE Trans. Pattern Anal. Mach. Intell.*, vol. 24, no. 5, pp. 603-619, 2002.
- [12] L. Pizarro, P. Mrazek, S. Didas, S. Grewening, and J. Weickert, "Generalised Nonlocal Image Smoothing," *Int. J. Comput. Vis.*, vol. 90, no. 1, pp. 62-87, 2010.
- [13] A. Buades, B. Coll, and J-M. Morel, "Neighborhood filters and PDE's," *Numer. Math.*, vol. 105, no. 1, pp. 1-34, 2006.
- [14] G. Gilboa and S. Osher, "Nonlocal Linear Image Regularization and Supervised Segmentation," *Multiscale Model. Simul.*, vol. 6, no. 2, pp. 595-630, 2007.
- [15] O. Lezoray, A. Elmoataz, and S. Bougleux, "Graph Regularization for Color Image Processing," *Comput. Vis. Image Underst.*, vol. 107, no. 1-2, pp. 38-55, 2007.
- [16] A. Wedel, D. Cremers, T. Pock, and H. Bischof, "Structure- and Motion-adaptive Regularization for High Accuracy Optical Flow," in *Proc. Int. Conf. Comput. Vis.*, pp. 1663-1668, 2009.
- [17] A. Elmoataz, O. Lezoray, and S. Bougleux, "Nonlocal Discrete Regularization on Weighted Graphs: A Framework for Image and Manifold Processing," *IEEE Trans. Image Process.*, vol. 17, no. 7, pp. 1047-1060, 2008.
- [18] M. Felsberg, P-E. Forssen, and H. Schar, "Channel Smoothing: Efficient Robust Smoothing of Low-Level Signal Features," *IEEE Trans. Pattern Anal. Mach. Intell.*, vol. 28, no. 2, pp. 209-222, 2006.
- [19] D. Barash, "A Fundamental Relationship between Bilateral Filtering, Adaptive Smoothing, and the Nonlinear Diffusion Equation," *IEEE Trans. Pattern Anal. Mach. Intell.*, vol. 24, no. 6, pp. 844-847, 2002.
- [20] A. Singer, Y. Shkolnisky, and B. Nadler, "Diffusion Interpretation of Nonlocal Neighborhood Filters for Signal Denoising," *SIAM J. Imaging Sci.*, vol. 2, no. 1, pp. 118-139, 2009.

- [21] M. Elad, "On the Origin of the Bilateral Filter and Ways to Improve It," *IEEE Trans. Image Process.*, vol. 11, no. 10, pp. 1141-1151, 2002.
- [22] D. Barash and D. Comaniciu, "A Common Framework for Nonlinear Diffusion, Adaptive Smoothing, Bilateral Filtering and Mean Shift," *Image and Vis. Comput.*, vol. 22, no.1, pp. 73-81, 2004.
- [23] P. Milanfar, "A Tour of Modern Image Filtering," *IEEE Signal Process. Mag.* (accepted)
- [24] E. P. Simoncelli and H. Farid, "Steerable Wedge Filters for Local Orientation Analysis," *IEEE Trans. Image Process.*, vol. 5, no. 9, pp. 1377-1382, 1996.
- [25] S. Paris and F. Durand, "A Fast Approximation of the Bilateral Filter Using a Signal Processing Approach," *Int. J. Comput. Vis.*, vol. 81, no. 1, pp. 24-52, 2009.
- [26] L. Sevilla-Lara and E. Learned-Miller, "Distribution Fields for Tracking," in *Proc. IEEE Conf. Computer Vision and Pattern Recognition*, pp. 1910-1917, 2012.
- [27] M. Aubry, S. Paris, S. W. Hasinoff, J. Kautz, and F. Durand, "Fast and Robust Pyramid-based Image Processing," MIT-CSAIL-TR-2011-049, 2011.
- [28] B. Ham, D. Min, and K. Sohn, "Robust Scale-Space Filter Using Second-Order Partial Differential Equations," *IEEE Trans. Image Process.*, vol. 21, no. 9, pp. 3937-3951, 2012.
- [29] F. Voci, S. Eiho, N. Sugimoto, and H. Sekibuchi, "Estimating the Gradient in the Perona-Malik Equation," *IEEE Signal Process. Mag.*, vol. 21, no.3, pp. 39-65, 2004.
- [30] S. T. Acton, "Locally Monotonic Diffusion," *IEEE Trans. Signal Process.*, vol. 48, no. 5, pp. 1379-1389, 2000.
- [31] K. Krissian and S. Aja-Fernandez, "Noise-Driven Anisotropic Diffusion Filtering of MRI," *IEEE Trans. Image Process.*, vol. 18, no. 10, pp. 2265-2274, 2009.
- [32] F. Durand and J. Dorsey, "Fast Bilateral Filtering for the Display of High-Dynamic-Range Images," *ACM Trans. Graph.*, vol. 21, no. 3, pp. 257-266, 2002.
- [33] J. Gosme, C. Richard, and P. Goncalves, "Adaptive Diffusion as a Versatile Tool for Time-Frequency and Time-Scale Representations Processing: A Review," *IEEE Trans. Signal Process.*, vol. 53, no. 11, pp. 4136-4146, 2005.
- [34] J. Weickert, "Coherence-Enhancing Diffusion Filtering," *Int. J. Comput. Vis.*, vol. 31, no. 2-3, pp. 111-127, 1999.
- [35] D. Tschumperle and R. Deriche, "Vecotr-Valued Image Regularization with PDEs: A Common Framework for Different Applications," *IEEE Trans. Pattern Anal. Mach. Intell.*, vol. 27, no. 4, pp. 506-517, 2005.
- [36] J. E. Kyprianidis, H. Kang, and J. Döllner, "Image and Video Abstraction by Anisotropic Kuwahara Filtering," *Computer Graphics Forum*, vol. 28, no. 7, pp. 1955-1963, 2009.
- [37] J. E. Kyprianidis and H. Kang, "Image and Video Abstraction by Coherence-Enhancing Filtering," *Computer Graphics Forum*, vol. 30, no. 2, pp. 593-602, 2011.
- [38] <http://www.kyprianidis.com/projects.html>
- [39] S. D. Zeno, "A Note on the Gradient of a Multi-Image," *Computer Vision, Graphics, and Image Processing*, vol. 33, pp. 116-125, 1986.
- [40] J. Zhang, J. Zheng, and J. Cai, "A Diffusion Approach to Seeded Image Segmentation," in *Proc. IEEE Conf. Computer Vision and Pattern Recognition*, pp. 2125-2132, 2010.
- [41] J. Weickert, "Theoretical Foundations of Anisotropic Diffusion in Image Processing," *Computing, Suppl.*, vol. 11, pp. 221-236, 1996.
- [42] J. Weickert and T. Brox, "Diffusion and Regularization of Vector- and Matrix-Valued Images," *Inverse Problems, Image Analysis, and Medical Imaging Providence*, Contemporary Mathematics, vol. 313, pp. 251-268, 2002.
- [43] G. Papari, N. Petkov, and P. Campisi, "Artistic Edge and Corner Enhancing Smoothing," *IEEE Trans. Image Process.*, vol. 16, no. 10, pp. 2449-2462, 2007.



Bumsub Ham (S'09) received the B.S. degree in electrical and electronic engineering from Yonsei University, Seoul, Korea, in 2008. He is currently pursuing the joint M.S. and Ph.D. degree at Yonsei University. He is mainly interested in variational methods and PDEs to solve 3D computer vision and image processing problems, particularly stereo vision, 3-D modeling, super-resolution, and HDR imaging.



Dongbo Min (M'09) received the B.S., M.S., and Ph.D. degree in electrical and electronic engineering from Yonsei University, Seoul, Korea, in 2003, 2005, and 2009, respectively. He then worked with the Mitsubishi Electric Research Laboratories (MERL) as a post-doctoral researcher from June 2009 to June 2010. He is now working with the Advanced Digital Sciences Center (ADSC), which was jointly founded by the University of Illinois at Urbana-Champaign (UIUC) and the Agency for Science, Technology, and Research (A*STAR), a Singapore government agency. His research interests include 3D computer vision, video processing, 3-D modeling, and hybrid sensor systems.



Kwanghoon Sohn (M'92) received the B.E. degree in electronic engineering from Yonsei University, Seoul, Korea, in 1983, the MSEE degree in electrical engineering from University of Minnesota in 1985, and the Ph.D. degree in electrical and computer engineering from North Carolina State University in 1992. He was employed as a senior member of the research staff in the Satellite Communication Division at Electronics and Telecommunications Research Institute, Daejeon, Korea, from 1992 to 1993 and as a postdoctoral fellow at the MRI Center in the Medical School of Georgetown University in 1994. He was a visiting professor at Nanyang Technological University from 2002 to 2003. He is currently a professor in the School of Electrical and Electronic Engineering at Yonsei University. His research interests include three-dimensional image processing, computer vision and image communication. Dr. Sohn is a member of IEEE and SPIE.